

<https://doi.org/10.1038/s44454-025-00020-2>

A self-cleaning, bio-inspired high retention filter for a major entry path of microplastics

Check for updates

Leandra Hamann ¹ ✉, Christian Reuß^{1,2}, Hendrik Herzog ¹, Kristina Schreiber ^{1,3}, Christian Geitner ⁴ & Alexander Blanke ¹

Microplastic (MP) fibres from washing machines are a major source of environmental pollution, yet, existing domestic filtration solutions are prone to clogging and have limited retention. Inspired by the gill arch system of ram-feeding fishes, we developed a bio-inspired filter that employs semi-cross-flow filtration with a conical filter element geometry, periodic self-cleaning and optimised inflow. Laboratory tests show that the fish-inspired filter (FiF) retains up to 99.6% of MP test fibres. Clogging is reduced by collecting up to 85% of the fibres outside the FiF through a periodic cleaning mechanism. CFD and flow tank experiments demonstrate that filtration performance is strongly influenced by the angle of attack and inlet geometry. The FiF achieves a low concentrate volume (~5%), increasing yield and minimising post-treatment. Our findings highlight the potential of bio-inspired filtration mechanisms for engineering applications such as washing machines requiring high efficiency and modular design.

Microplastics (MPs), plastic particles and fibres smaller than 5 mm, are ubiquitous pollutants found in water¹, soil² and air³. In all these environments, MPs have adverse effects, for example, they accumulate fungal pathogens in soil⁴, cause phytotoxicity on vascular plants⁵, enter marine top predators through trophic transfer⁶, and induce oxidative stress, inflammation, and metabolic disorders in humans⁷. It is widely acknowledged that a diverse combination of mitigation strategies is necessary to reduce MPs from entering the environment. Long-term strategies include shifting to a circular economy, developing new materials and sustainable products, and conducting educational work to change societal mindset^{8–10}. Short-term measures include, for example, legislation to ban MPs in cosmetics, the use of substitute materials, or cleaning activities^{11,12}. Filtration is another short-term means to reduce MPs close to their sources and entry points, but current filtration solutions are hindered by low retention efficiencies for MPs, as well as rapid clogging.

Washing machines are a major entry path for MPs, releasing between 10 and 120 g of MP fibres from textiles per person per year, and are one of the major MP sources^{13–15}. Washing machines have coarse filters to protect the pump by retaining stones or coins, but no MP filter¹⁶. Hence, MPs are brought unfiltered into the sewage system. Wastewater treatment plants equipped with secondary and tertiary treatment stages retain 84–94% of MPs¹⁷. However, retained MPs accumulate in the sewage sludge, with 63–90% coming from washing machines¹⁷. The MPs are then reintroduced

into the environment when the sewage sludge is disposed of on agricultural fields, as is common practice globally^{17,18}. Therefore, despite the high retention rates within wastewater treatment plants, intercepting MPs before they reach the sewage system is a critical and underdeveloped intervention point.

We present a biomimetic, fish-inspired filter (FiF) with high filtration efficiency of standardised MP fibres and a self-cleaning process. Our filter module is based on the filter-feeding process in ram-feeding fishes because aspects of this filtration process, in principle, fits some of the requirements in washing machines such as particle size, flow regime, and filter size (Supplementary Note 1 and Supplementary Fig. 1). Ram-feeding fishes are pelagic fishes that use their forward motion to induce flow through the gill arch system^{19,20}. The gill arch system is composed of gill arches with elongated gill rakers. The morphology of the gill arch system is species dependant with some having denticles on the gill arches and gill rakers¹⁹, while others produce mucus to accumulate particles²¹, have surface structures that induce local vortices to retain particles²² or use a combination thereof. In most filter-feeding fishes, the gill arches form a cone-shaped geometry that tapers down towards the oesophagus within the buccal cavity^{19,23–25}. While swimming forward with an open mouth, a tangential flow transports the food particles towards the oesophagus, and the cleared water exits between the gill arches and under the operculum. This process was previously described as cross-flow filtration with variations found in some species called cross-step filtration^{20,22}. Based on morphology and video analysis of their feeding behaviour¹⁹, it is

¹Bonn Institute for Organismic Biology, University of Bonn, Bonn, Germany. ²DSG-Canusa GmbH, Development Engineer, Rheinbach, Germany. ³Biomimetics Group, Energy and Sustainability Research Institute, University of Groningen, Groningen, The Netherlands. ⁴Fraunhofer Institute for Environmental Safety and Energy Technology UMSICHT, Oberhausen, Germany. ✉e-mail: hamannleandra@gmail.com

likely that the filtration process in ram-feeding fish like anchovy, pilchard, and Atlantic mackerel, in fact, combines cross-flow and dead-end filtration. In these fishes, the gill rakers form a flat surface that induce particles rolling towards the oesophagus where they accumulate before being swallowed¹⁹. Particle rolling is enabled by the conically tapered geometry of the gill arch system. The geometry is described by an angle of attack α (Fig. 1A), and may range between 0°(dead-end filtration) and 90°(cross-flow filtration, Fig. 1B). Therefore, the filtration process was previously called semi-cross-flow filtration¹⁹ (Fig. 1B). Our FiF mimics the functional morphology in selected ram-filter-feeding fishes to take advantage of the semi-cross-flow filtration process. Furthermore, by varying parameters like filter size, mesh size or angle of attack in physical and numerical experiments, we demonstrate that filter performance depends on specific parameter combinations and can thus be tailored to a wide range of potential applications, including retention of MPs in washing machines. Our fish-inspired filter (FiF) is unique in its combination of (i) a cone-shaped filter element with a filter medium at a set angle of attack α to induce semi-cross-flow filtration, (ii) a filter housing with adapted inflow and separate permeate and concentrate outlet, and (iii) an adjustable periodic cleaning mechanism that delays clogging.

Results

Effect of angle of attack on particle deposition during semi-cross-flow filtration

The gill arch system inside the buccal cavity is tapered towards the oesophagus, bilaterally symmetric, and consists of five gill arches that bear

elongated gill rakers with denticles forming a mesh (Fig. 1A). In micro-CT scans of five ram-feeding fishes, the angle of attack α was measured between the hyoid bone and an extended line of the GR of the first four arches in virtual cross-sections of the fish’s head (Fig. 1A). Across all five species, α ranged between 4° for more anterior and 47° for more posterior gill arches (Supplementary Fig. 2). Based on the semi-cross-flow filtration process¹⁹, this would indicate that particles entering the fish’s mouth would experience higher tangential forces at lower α at the more anterior gill arches. Consequently, particles would roll along the gill rakers and denticles so that they accumulate close to the oesophagus due to higher α before being swallowed (Fig. 1A, B). In order to test this hypothesis, we observed particle rolling on filter meshes at α ranging from 0° to 60° under a range of other parameter variations in a series of flow tank experiments. We found that the share of rolling MP and non-MP particles —with no ‘permanent’ deposition and potential clogging of the filter mesh- increases with lower α , but the strength of that effect varies with particle type and mesh size (Fig. 1C). Round brine shrimp eggs, a part of the natural food of ram-feeding fishes, keep rolling up to an angle of 40° after which the probability to roll drops and reaches <30% at 60°. Brine shrimp adults show a similarly high probability to roll at low angles but a more linear decrease with higher α . The probability of rolling for MP fragments decreases in a cubic relation and is generally lower than for the natural particles. The probability of rolling is overall the smallest for the MP fibres compared to the other particle types. The probability of rolling drops from 20% at 10° to 0% at 40° with the 53 μm mesh size and from 37.5% at 10° to 0% at 50° with the 100 μm mesh size. With the 300 μm mesh size,

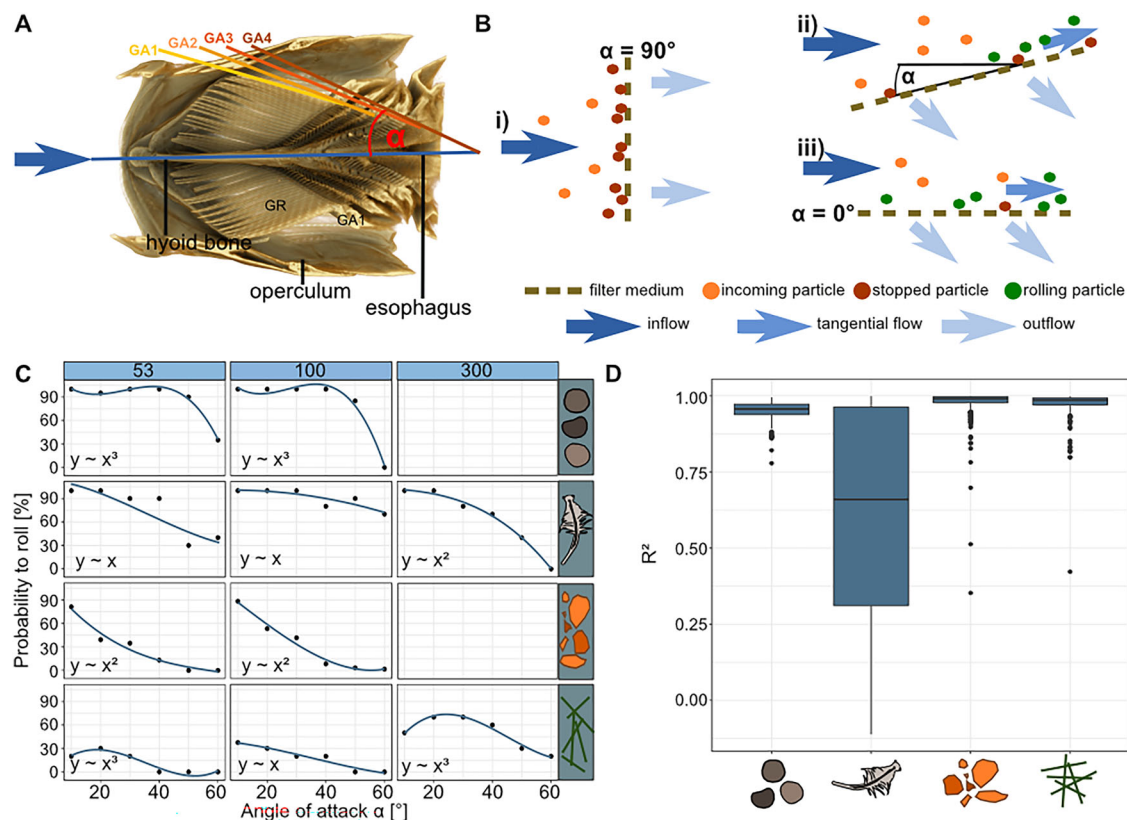


Fig. 1 | Interaction of particles with filter media at different angles of attack. A Volume render cross-section through the frontal plane with view on the ventral side of the buccal cavity of Micro-CT scans the Indian mackerel *Rastrelliger kanagartha*. The blue arrow and blue line indicate the inflow and midline of the fish, and one side of α . The yellow, orange and red lines indicate the orientation of the four gill arches (GA1-4) and the other side of α . **B** Schematic drawing of (i) dead-end filtration with $\alpha = 90^\circ$, (ii) semi-cross-flow filtration with α ranging between 0° and 90°, and (iii) cross-flow filtration with $\alpha = 90^\circ$. Depending on inflow and the α of the filter medium, the tangential flow induces particles to stop or roll along the

surface of the filter medium. **C** Probability of particles rolling after contact with the filter medium for each α (10°–60°), particle type (Brine shrimp eggs, Brine shrimp adults, MP fragments, MP fibres), and mesh size (53, 100, 300 μm). Polynomial regression, with y on x , was used to describe the influence of α on the probability of rolling. There are no results for the brine shrimp eggs and MP fragments because the mesh size was too big to retain the smaller particles. **D** Boxplots of all R^2 of the Boltzmann fit to describe the motion of all four particle types. For more details of particle characteristics and results of preliminary experiments, see Table 2 and Supplementary Fig. 3.

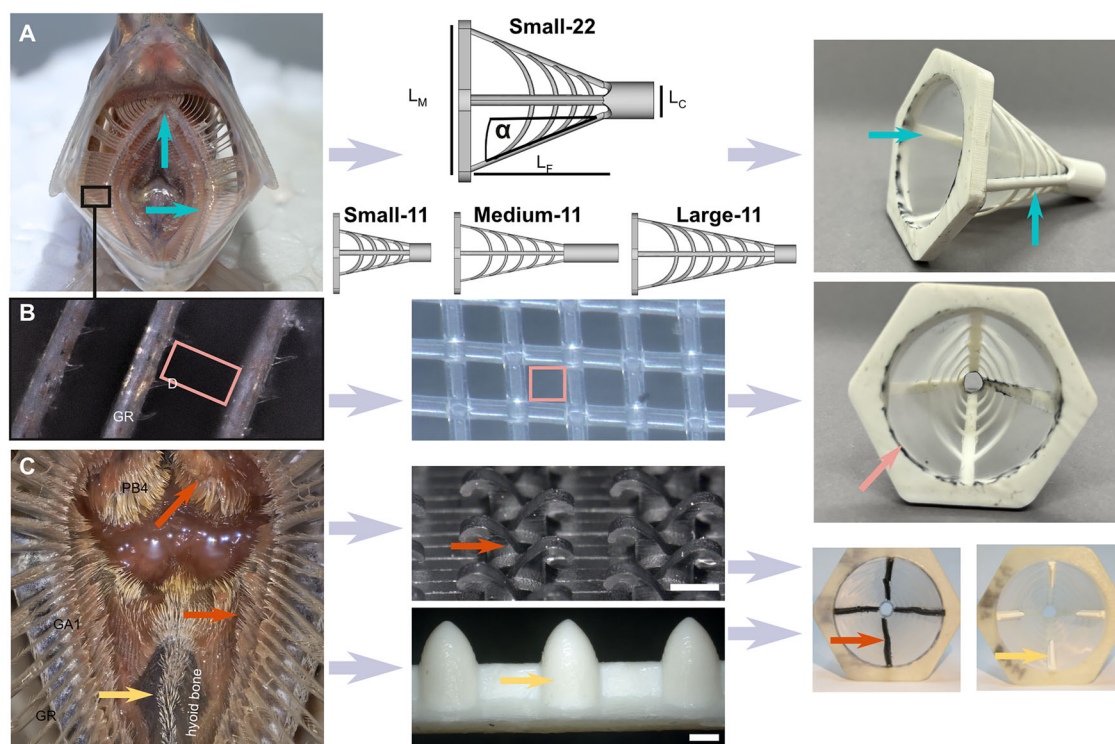


Fig. 2 | Abstraction of morphological traits of ram-feeding fishes into CAD models and physical models. **A** The cone-shaped gill arch system with a given angle of attack α is mimicked by the support structures of the filter elements (blue arrows). The filter element is described by an inflow opening diameter L_M and an outflow diameter L_C with a filter length of L_F and a total length of L_T . **B** The gill rakers (GR)

and denticles (D) form the meshes (red box) and are mimicked with a purchased filter mesh that is glued onto the support structures. **C** Surface structures as observed in ram-feeding scombrids are mimicked by a row of ellipsoids that mimic the short GR, and hooked tape mimics the denticles and teeth, and is glued in the Large-11 filter element.

the probability of rolling first increases from 50% at 10° to 70% at 20° and then decreases to 20% at 60° (Fig. 1C). Another difference between the brine shrimp adults in comparison to the brine shrimp eggs and MPs is the quality of the Boltzmann fit to the velocity profile of the particles when in contact with the filter mesh (Supplementary Fig. 3). For the brine shrimp adults, R^2 is 0.60 ± 0.34 whereas it is 0.95 ± 0.03 , 0.97 ± 0.05 , and 0.98 ± 0.06 for the brine shrimp eggs, MP fragments and MP fibres, respectively (Fig. 1D). This indicates a different behaviour of the motile brine shrimp adults in comparison to the other, non-motile particles. Hence, for MP retention, the angle of attack should preferably be lower than 20° to keep the MPs in suspension or rolling for longer and reduce clogging of the filter medium.

Design of fish-inspired filter element

In order to design a filter that separates particles based on semi-cross-flow filtration, we mimicked the gill arch system morphology with the filter element. The basic design of a filter element is radially symmetric and has several arched support structures that resemble the gill arches and can hold commercially available and standardised filter meshes (Fig. 2A, B). The filter mesh creates a flat filter medium as observed in the Atlantic herring, the Atlantic pilchard, and the Atlantic anchovy formed by the gill rakers and denticles (Fig. 2B). The filter element is described by an inflow opening, resembling the mouth, with diameter L_M and an outflow opening, resampling the oesophagus, with diameter L_C and a filter length of L_F (Fig. 2A). Since $L_M > L_C$, the gill arches and the associated mesh decrease in diameter, which results in the angle of attack, α . By changing the filter element length or the opening diameter, α can be adjusted to lower or higher angles to increase particle rolling towards the outflow opening, while clean fluid exists laterally through the mesh. Overall, we built four different filter elements that covered three different length, i.e. small, medium and large, and two α , i.e. 11° and 22° (Table 1). Some of the species, i.e. Atlantic mackerel and Indian mackerel, also show shortened gill rakers and teeth that point inwards into the buccal cavity (Fig. 2C). These structures were mimicked by

the hooked side of Velcro or 3D printed row of ellipsoids that can optionally be added inside any of the filter elements. For comparing the FiF element to a conventional dead-end filter design, one filter element had an α of 0° and no outflow opening. The length was chosen so that the filtration area A_F was kept similar to the Large-11 filter elements to allow comparisons of these different designs (Table 1).

Integration into a functional filter housing

The filter element was encased in a filter housing consisting of an inlet, a flange, a transparent pipe for visual inspection, and an outlet (Fig. 3A, B). The outlet has two outlet pipes to separate the clean fluid that exits laterally through the filter element, i.e. the permeate (V_P) with potentially lost MPs (M_P), and the drainage of concentrate (V_C) through the outflow opening that contains the accumulated particle mass (M_C). Both outlet pipes are equipped with automated valves to mimic the periodic cleaning and swallowing in the fishes. During filtration mode, the concentrate valve is closed and the permeate valve is open which accumulates particles in the filter element and allows outflow of cleaned water through the mesh. For cleaning of the filter, the permeate valve closes while the concentrate valve opens so that the fluid with the particles is directed out of the concentrate outlet and the filter element is cleaned, here shown with MP fibres (Fig. 3C, D). In the fishes, periodic cleaning, i.e. swallowing, was observed in intervals between 0.17 s in the Atlantic herring, 0.27 s in the Atlantic herring, 0.53 s in the Atlantic mackerel and 3.7 s in the Indian mackerel¹⁹. For the FiF experiments, the cleaning intervals were set to clean after half of the test suspension passed and right before the total test suspension passed. Since volume flow depends on filter size and inlet type (Supplementary Fig. 5), the cleaning intervals were adjusted according to the particular filter setup and ranged between 0.6 s and 1.3 s.

To investigate whether the inlet design and different cleaning setups will influence the flow patterns inside the filter element, we tested two different inlet geometries and two cleaning modes using computational fluid

Table 1 | Overview of four filter elements used in the FiF and a dead-end filter for comparison

	Small-22	Small-11	Medium-11	Large-11	Dead-end
Filter length L_F [mm]	62.6	52.7	77.7	102.7	60.8
Angle of attack α [°]	22	11	11	11	0
Inner diameter at inlet d_M [mm]	50	30.5	40.3	50	50
Inner diameter of outlet d_C [mm]	10	10	10	10	0
Filtration area A_F [mm ²]	5075.4	3415.5	6248.0	9861.1	9860.0

The filter mesh inside each element is not shown here.

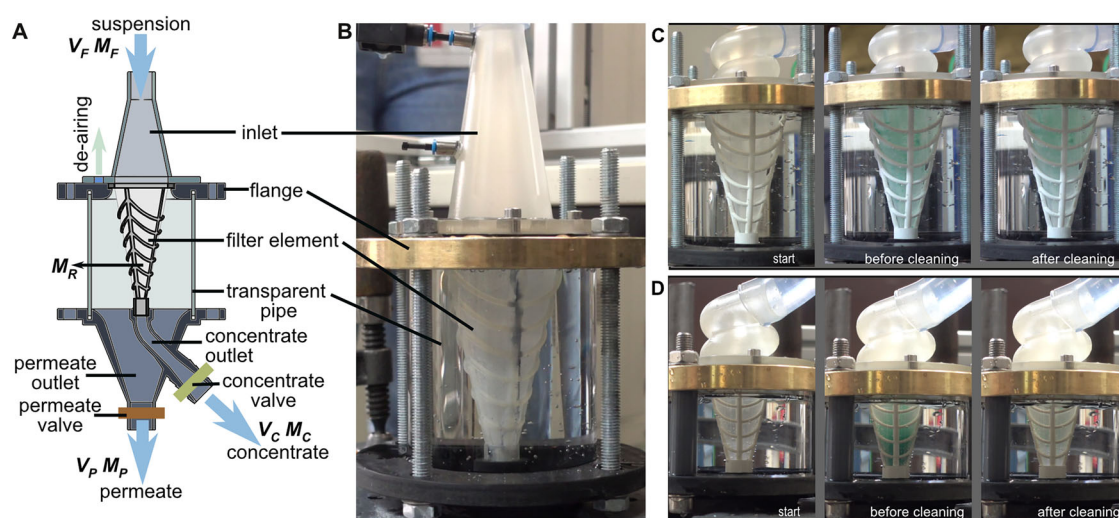


Fig. 3 | Design of the filter housing and cleaning mechanism. **A** The modular filter housing consists of an inlet with a screw to de-air the system, a flange, a transparent pipe, and the outlet with a separation of concentrate and permeate. The FiF separates the feed suspension, which consists of a fluid volume (V_F) and a particle mass (M_F), into a concentrate volume (V_C) with a particle mass fraction (M_C) and the clean permeate (V_P) with a second particle mass fraction (M_P). The particle mass fraction that remains in the filter element is called the

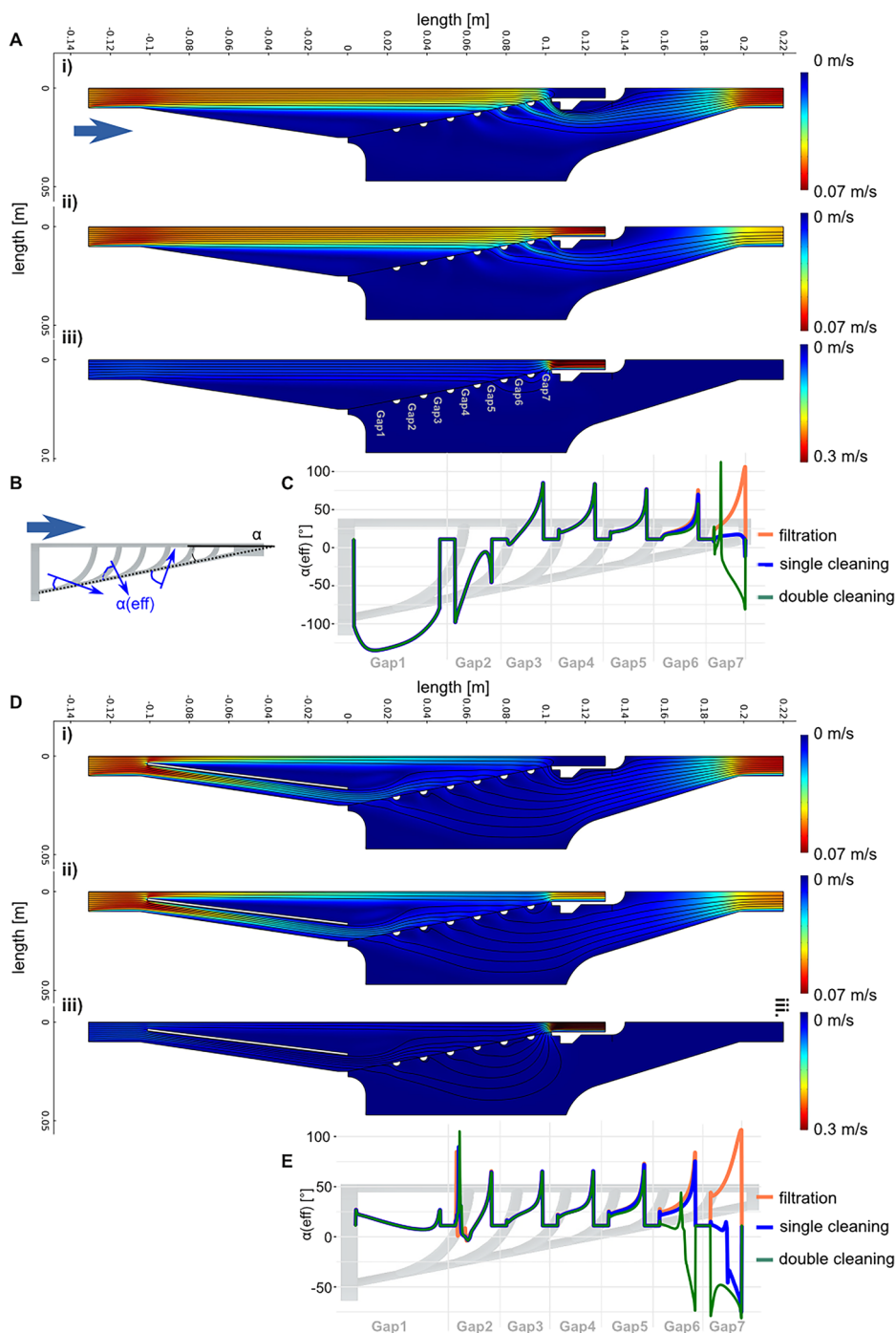
retentate (M_R). The cleaning mechanism is regulated by the permeate valve and the concentrate valve at the respective outlets. **B** Set-up of the FiF with the long inlet and the Large-11 filter element. **C** Observations of MP fibres in the Large-11 filter element with the snail inlet at the start of the experiment, before cleaning, and after cleaning. **D** Observations of MP fibres in the Small-11 filter element with the snail inlet at the start of the experiment, before cleaning and after cleaning.

dynamics (CFD) (Fig. 4). The geometry consisted of a rotational symmetric Large-11 filter element. To quantify the effects on the flow, we measured the effective angle of attack $\alpha(\text{eff})$. While the angle of attack α is defined by the filter element geometry and remains static, $\alpha(\text{eff})$ is the resulting angle by the streamlines at contact with the filter mesh when the flow exits laterally through Gap 1–Gap 7 (Fig. 4B). A lower positive $\alpha(\text{eff})$ should result in flatter, more parallel streamlines towards the filter mesh and, hence, further increase the probability of rolling for any particles that follow the streamlines.

The CFD results reveal that the presence of an internal wall in the inlet alters the local flow field and improves $\alpha(\text{eff})$ at the filter mesh, especially at Gap1 and Gap2 (Fig. 4Ai, Di). Without the internal wall, the incoming flow is not deflected but hits the filter mesh in a straight line and creates a recirculation zone with backflow through Gap 1 and Gap 2 indicated by negative $\alpha(\text{eff})$ (Fig. 4C, E and Supplementary Fig. 4). This dead zone reduces the effective filtration area, potentially leading to uneven particle accumulation

and a less favourable flow distribution for semi-cross-flow filtration. In contrast, the internal wall guides the flow more uniformly along the filter surfaces, thereby leading to a low, but still positive $\alpha(\text{eff})$. Besides the filtration mode (permeate outlet open, concentrate outlet closed, Fig. 4Ai, Di), we also tested two cleaning modes, i.e. single cleaning (permeate outlet open, concentrate outlet open, Fig. 4Aii, Dii) and double cleaning (permeate outlet closed, concentrate outlet open, Fig. 4Aiii, Diii). The three operating modes have a significant impact on the local flow orientation near the concentrate outlet. During both cleaning modes, backflow forms at Gap 6 and Gap 7, leading to a negative $\alpha(\text{eff})$ (Fig. 4C, E). This effect is especially strong in the double cleaning mode and may be beneficial for the FiF’s performance. The reverse-throughflow could detach particles adhering to the filter mesh and flush them towards the concentrate outlet. As positive $\alpha(\text{eff})$ increases from Gap 1 to Gap 7 during the filtration mode, most particles will likely deposit in the posterior region during semi-cross-flow filtration. Consequently, this backflushing effect may be particularly advantageous at these gaps to prevent clogging.

Fig. 4 | Flow through a 2D half of the FiF with a Large-11 filter element using computational fluid dynamics (CFD) in COMSOL®. We compared the influence on flow behaviour of a long inlet (9° angled) with (A) no inner wall and D an inner wall during the three operating modes: (i) the concentrate outlet is closed and the permeate outlet is open (filtration mode), (ii) the concentrate outlet is open and the permeate outlet is open (single cleaning mode) and (iii) the concentrate outlet is open and the permeate outlet is closed (double cleaning mode). The support structured and gaps between the support structures of the filter elements are exemplarily indicated in Fig. Aiii). The light blue arrow indicates the direction of flow. **B** The angle of attack α (black, Aiii) is given by the filter element, whereas the effective angle of attack $\alpha(\text{eff})$ changes depending on the orientation of the streamlines in relation to filter mesh (blue). Note that the colour scale indicating flow velocity is the same in (i) and (ii) but differs in (iii). The change of $\alpha(\text{eff})$ at the filter mesh over the full length of the filter element for each operation mode is plotted for the setup with (C) no inner wall and E inner wall. The support structures of the filter elements are shown in grey with the separation into the seven gaps. The negative $\alpha(\text{eff})$ values in (C) are caused by a recirculating vortex created across the filter element and reversed streamlines at gap1 (Supplementary Fig. 4).



Proof of concept of the fish-inspired filter

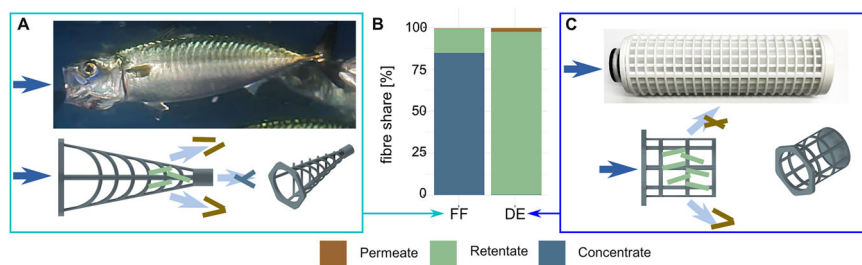
Our FiF retains $99.6 \pm 0.8\%$ of MP fibres in the lab experiments (Fig. 5A, B). While this filtration efficiency E_R is similar compared to the filter design based on dead-end filtration with $97.7 \pm 3.1\%$ for the same filtration area, our FiF delays clogging through a cone-shaped geometry in combination with a periodic cleaning mechanism, and collects up to $84.8 \pm 3.5\%$ of the retained 2 mm MP fibres, outside of the FiF in the concentrate (concentrate filtration efficiency E_C). In the FiF with a conical-shaped filter element and an angle of attack $\alpha = 11^\circ$, the concentrate is collected through an outlet at the terminal end (Fig. 5A). The concentrate contained only 850 ml, i.e. 4.25% of the filtered fluid volume. At the same time, $14.3 \pm 3.7\%$ of the MP fibres remain as retentate in the filter element, which is approximately one seventh of the MP fibres in the filter element of the dead-end filter. In the

dead-end filter, no MP fibres are collected outside the filter element as it has no concentrate outlet and all fluid has to pass the filter medium, which is typical for example in cartridge filters (Fig. 5C). This comparison shows that our FiF keeps the MP fibres rolling or in suspension, prevents the accumulation of MP fibres in the filter itself, and allows removal of the MP fibres through periodic cleaning. The majority of MP fibres are collected in the concentrate outside the FiF.

Parameter adaptation for the application in washing machines

Based on the conditions found in washing machines, a filter should fit the available space in the washing machine housing, not add additional drag for the pump, withstand changing volume flow and flow velocities, and have high filtration efficiencies (see washing machine requirements in

Fig. 5 | Comparison of the fish-inspired filter (FiF) with a dead-end (DE) filter element. **A** Atlantic mackerel *Scomber scombrus* with open mouth during filter-feeding and CAD design of the Large-11 FiF element. **B** Performance comparison of the DE and FiF filter element design based on MP fibre share in permeate, retentate and concentrate. **C** Common engineered filter cartridge of a MP washing machine filter and computer-aided design (CAD) of a filter element based on that design with the same filtration area as the FiF element. For filter element dimensions, see Table 1.



Supplementary Note 1). FiF performance was evaluated on three parameters: filtration efficiency of MP fibres retained in the FiF (E_R), i.e. the concentrate and retentate, MP fibres retained in the concentrate (E_C), and yield in concentrate (η_C), which includes the fibre mass in the concentrate (M_C) and the concentrate volume (V_C). Yield in concentrate is especially relevant for applications in washing machines, because a small concentrate fluid volume is preferable to reduce post-treatment and user interaction.

First, we decreased the initially designed filter element length L_F of 102.7 mm (large) and designed two smaller sizes of 77.7 mm (medium) and 52.7 mm (small) (Table 1). Even though a lower α would increase particle rolling, the length of the filter and therefore α is limited by the available space in the washing machine. Therefore, we kept $\alpha = 11^\circ$ (denoted by '11' in 'Large-11', 'Medium-11' and 'Small-11' filter types) as presented in the initial experiment to compare the FiF with the dead-end filter (Fig. 5). While E_R remains relatively similar in Large-11 with $93.2 \pm 2.8\%$, Medium-11 with $94.0 \pm 4.2\%$ and Small-11 with $96.0 \pm 5.5\%$, the MP fibre share in the concentrate E_C increased from $35.0 \pm 12.6\%$, to $50.6 \pm 9.4\%$ in Medium-11 up to $65.3 \pm 13.7\%$ in Small-11 (Fig. 6A). The yield in concentrate η_C also slightly increased with $83.2 \pm 6.5\%$ in Large-11, $84.9 \pm 10.3\%$ in Medium-11 and $88.8 \pm 15.3\%$ in Small-11.

When increasing α to 22° in the Small filter element ('Small-22'), we observed that E_R decreased from $96.0 \pm 5.5\%$ to $84.5 \pm 6.7\%$, E_C decreased from $65.3 \pm 13.7\%$ to $37.9 \pm 14.8\%$, and η_C decreased from $88.8 \pm 15.3\%$ to $62.0 \pm 14.8\%$ (Fig. 6B), suggesting that a larger angle of attack may adversely affect performance.

As there are not only MP fibres of different sizes in the washing machine effluent, but also sand, dust, pollen, hair and detergents (Supplementary Note 1), we tested three mesh sizes (53, 78 and $100 \mu\text{m}$) for the Large-11 and two mesh sizes (53 and $100 \mu\text{m}$) for the Small-11 (Fig. 6C). Although mesh size is expected to influence filtration performance parameters, the changes showed no trend related to an increase or decrease in mesh size (Fig. 6C).

To verify the influence of different inlet geometries on filtration performance, as was indicated by the CFD experiments, we tested the long inlet at 9° with an internal wall (long inlet), a swirl inlet with a helical internal wall and a snail inlet (Fig. 6D). The swirl inlet and the long inlet performed similarly with E_R being $96.0 \pm 5.5\%$ and $96.2 \pm 3.6\%$, E_C being $65.3 \pm 13.7\%$ and $66.8 \pm 7.8\%$, and η_C being $88.8 \pm 15.3\%$ and $89.9 \pm 9.4\%$, respectively. The snail inlet showed a less high E_R with $85.5 \pm 14.1\%$ and η_C with $67.4 \pm 23.0\%$, but E_C was slightly higher with $68.0 \pm 38.3\%$ (Fig. 6D).

We also investigated the relevance of surface structures on the inside of the filter element (Fig. 2C) because some fish species showed surface structures directed perpendicular to α (Fig. 2C). We fitted the Large-11 filter element with three different surface structure designs but the results suggest that these did not improve performance (Fig. 6E).

Discussion

The best-performing FiF combination, based on the lowest share of MP fibres in the permeate and the highest yield in concentrate, is the Large-11 filter element with a mesh size of $78 \mu\text{m}$, in combination with the swirl inlet. It retains over 99% of the MP fibres with $0.8 \pm 2.2\%$ left in the permeate (E_R , Fig. 6C). The yield in concentrate η_C is $97.5 \pm 5.6\%$. However, the best

performing FiF configuration based on MP fibre share in the concentrate is the Small-11 filter element with a mesh size of $53 \mu\text{m}$ in combination with the swirl inlet with $79.8 \pm 6.8\%$ (Fig. 6C). This may indicate that the cleaning mechanism covers a larger share of the filtration area in the Small-11 filter element. Specifically, the shear forces in semi-cross-flow filtration will move the particles along the filter mesh at a low α until they deposit near the concentrate outlet as observed in the Large-11 and Small-11 filter elements (Fig. 3C, D), similar to the forces in cross-flow filtration^{26,27}. Consequently, the reversed flow near the concentrate outlet during the double cleaning mode, as shown in the CFD simulations (Fig. 4), detaches more particles, flushes them out of the filter element, and increases the share of MP fibres in the concentrate. Both best performing FiFs used the swirl inlet, which might be due to the creation of a rotational, likely turbulent flow that further reduces the positive effective angle of attack $\alpha(\text{eff})$ laterally towards 0° so flow becomes more parallel to the filter medium. In cross-flow filtration, turbulent flow is preferred over laminar flow because it increases the shear rate and prevents particle deposition on the filter mesh²⁷. The poorest performing FiF combination is the Small-22 with E_R being $15.5 \pm 6.9\%$ and η_C of $62.0 \pm 14.8\%$. This indicates that a higher angle of attack substantially reduces the benefits of semi-cross flow filtration (Fig. 1).

Another advantage to cross-flow filtration is the low concentrate volume and, therefore, an increased yield in concentrate η_C . In established cross-flow ultra-, nano- and microfiltration processes, the concentrate volume ranges between 10% and 50% of the feed, depending on system design²⁸⁻³⁰. With the conical FiF and the periodic cleaning, we achieve a concentrate volume of $4.9 \pm 1.6\%$ of the feed across all FiF combinations ($N = 70$). A smaller concentrate volume lowers post-treatment or disposal costs, improves the cleaning efficiency, and reduces fouling through smaller stagnant volume and cake layer formation. Additionally, the FiF collects most of the MP fibres outside the filter housing, and only one seventh of the MP fibres remain in the filter element (Fig. 5B). This indicates that clogging may be delayed by up to a factor of seven. An increase in cleaning frequency could prolong the delay; however, this might come at the expense of a high fluid volume in the concentrate. A thorough cleaning in which the filtration process was set back to starting conditions was not observed as all FiF combinations still had some MP fibres remaining in the retentate (Fig. 6). During examination of the filter elements after the experiments, we noticed that some MP fibres were stuck in the pores in areas glued to the support structures. Remaining MP fibres may necessitate that the filter element be removed for cleaning, which is common practice in many filtration processes, such as dead-end filtration³¹. But since most MP fibres are collected outside and the dirt-holding capacity is not limited to the volume of the filter element, cleaning time and required energy are kept to a minimum. By collecting most MP fibres outside the FiF, wear on the filter medium from mechanical cleaning (e.g. scrapes or brushes) is reduced, helping to overcome a key limitation of conventional domestic filters³¹.

Besides the FiF presented here, other bio-inspired filtration processes also show potential for technical applications. The particle separator by Piedrahita et al.³² is inspired by cross-flow filtration in pump-feeding fish. In simulations, a maximum of about 70%³² and in experiments with prototypes, a maximum of 43% of particles were retained³³. The concept of 'ricochet separation' was discovered in manta rays by Divi et al.³⁴, which

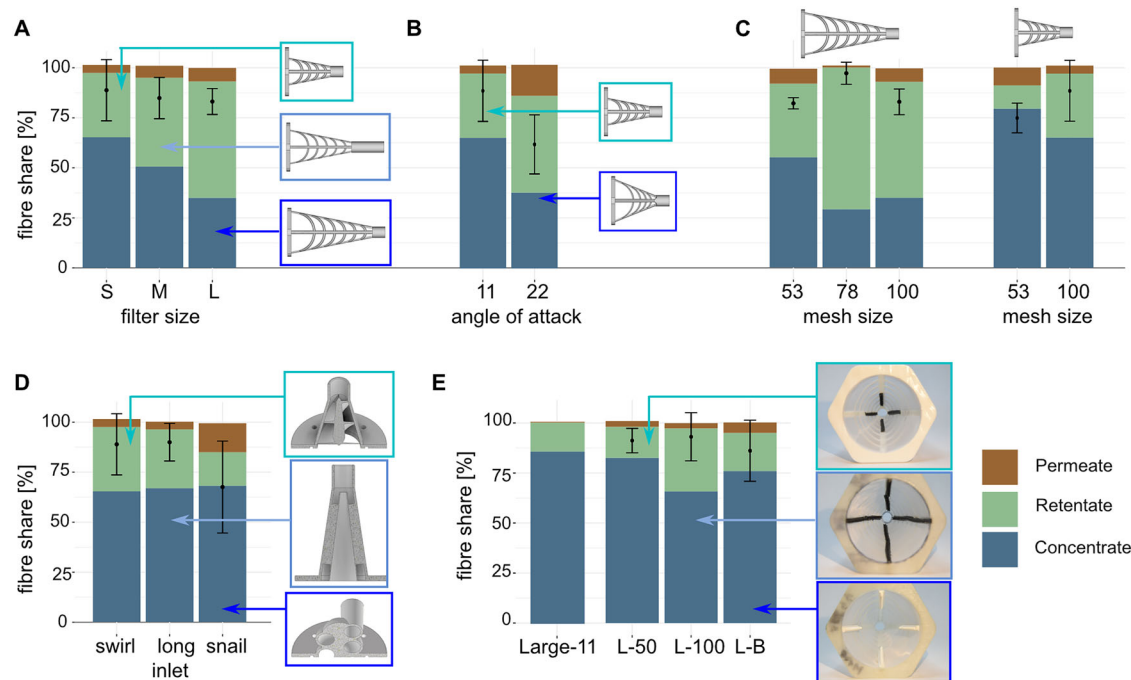


Fig. 6 | Filtration performance of the FiF (each $N = 5$) based on fibre share in permeate (brown), retentate (green), and concentrate (blue). Yield in concentration η_C is indicated by the mean with error bars (black). Variations include (A) filter size with Small-11 (S), Medium-11 (M) and Large-11 (L) filter element, snail inlet and mesh size 100 μm , B angle of attack α with the small filter element, snail inlet and mesh size 100 μm , C mesh size with the Large-11 (left) and Small-11 (right) filter element and snail inlet, D inlet type (swirl, long inlet at 9° with internal wall,

snail) with Small-11 filter element and mesh size 100 μm , and E bio-inspired surface structures on a Large-11 filter element (100 μm mesh size) with half way hooked tape (L-50), full way hooked tape (L-100) and bumpy structures (L-B), and the snail inlet. Surface structures made from hooked tape and 3D-printing mimic teeth and bumpy gill rakers found in ram-feeding mackerels (Fig. 2). Please note that the experiments presented in E were done with a different test volume and, therefore, cannot be directly compared to the other results.

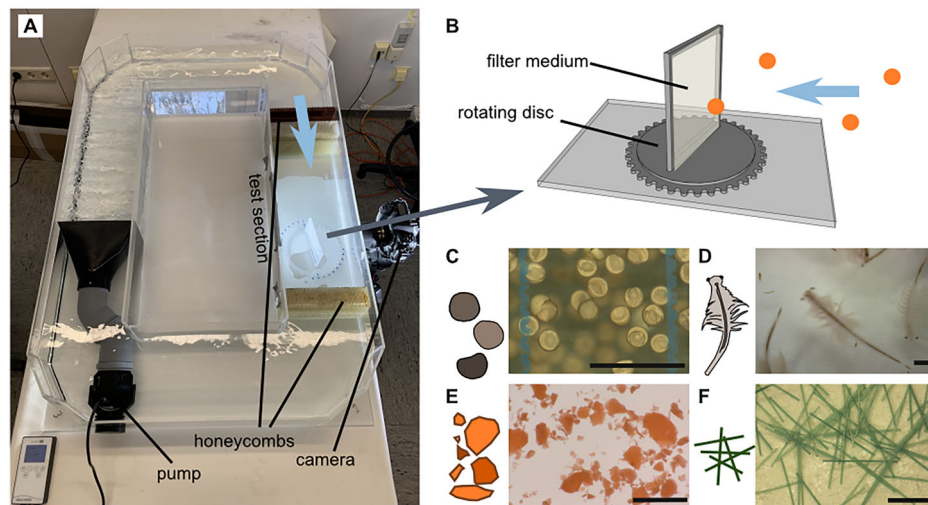
describes a mechanism in which particles bounce off the filter lobes, i.e. specialised gill rakers. A simplified filter lobe geometry was used to manufacture surface patterning on membranes to manipulate local flow fields and inhibit particle deposition³⁵. In small-scale experiments under cross-flow, the membranes with a pore size between 3.5 and 10.5 μm removed 97.6% of MP particles of 700 nm in diameter from water³⁶. In 2025, the filtration process was also virtually tested in CFD simulation for an application in fuel filtration, where it showed a significant reduction in pressure drop³⁷. The ‘cross-step filtration’ is another process found in ram-feeding fishes such as the American paddlefish and was first described by Sanderson et al.²³. The proof-of-concept was shown in abstracted models for the collection of harmful algae³⁸ and fibre collection in washing machines¹⁶. The commercial VORTX filter by CLEANR®, a spiral adaptation of this principle, reportedly achieves 90% efficiency for MP fibres $\geq 50 \mu\text{m}$, a 300% longer life and operates without a replaceable filter³⁹. While promising, its performance data are currently based on manufacturer claims and focus primarily on domestic washing machine applications. These examples reflect the diversity of bio-inspired filtration designs serving a wide range of applications—from nanoparticle removal to domestic washing machine filtration. This diversity not only highlights the versatility of biological inspiration but also demonstrates a growing demand for bio-inspired solutions to complex separation challenges. In this context, the FiF offers a valuable addition and represents an alternative route, particularly suited to applications requiring coarse fibre separation, low concentrate volumes, and modular cleaning systems.

Currently, the MP fibre length is larger than all tested mesh sizes and the rod-shaped MP fibres can only pass when they encounter the mesh perpendicularly. Smaller MP fibre sizes should be tested to see if the semi-cross-flow process also keeps smaller MP fibres in suspension or if a smaller mesh size is required. The cut-off size of retained MP fibres is a crucial value to determine if the FiF can compete with other washing machine filters. So far, it was suggested that a filter should retain $>80\%$ of MP fibres larger than

100 μm to be competitive^{40,41}. While conventional cross-flow filtration is typically applied to particle sizes below 10 μm using membrane-based systems (e.g. microfiltration or ultrafiltration), our tests with the large MP fibres show that the design extends semi-cross-flow filtration to the retention of larger, elongated fibres.

Fibre shape might also be a factor that influences filtration efficiency. The here used standardised MP fibres are rod-shaped, whereas textile fibres are of different lengths and irregularly shaped⁴². In the preliminary experiments, we could show that different particles show different recovery ratios and even the MP fibres with the best recovery ratio show a relatively high variance in the results (Supplementary Note 3). We suspect that a small share of MP fibres deposited somewhere in the setup. Resuspension could even contaminated the next experiment despite rinsing the test stand in between trials, because sometimes the sum of all fibres exceeded 100%. In contrast, we showed that lab contamination and scale accuracy did not have much influence (Supplementary Note 3). More computational methods, such as finite element modelling (FEM) and CFD can complement physical experiments with the biological model or engineered prototype, e.g. the stability and hydrodynamics of GR or the role of boundary layers around denticles in mesh formation. Though the CFD experiments were not used to verify the physical experiments but as supplementing method, they increased the understanding of flow patterns during semi-cross-flow filtration under changing geometries and filtration modes (Fig. 4). Based on these results, we would also expect that $\alpha(\text{eff})$ will increase more evenly from inlet to concentrate outlet when the support structures are not present. This could be achieved, for example, through the use of a stainless steel filter mesh that is rigid enough to maintain its conical shape. However, the results must be interpreted with certain limitations in mind. The numerical model was implemented as a two-dimensional, rotationally symmetric approximation of the actual filter geometry and the simulations were conducted under steady-state conditions with water as a homogeneous Newtonian fluid. In real-world applications such as washing machines, flow conditions may

Fig. 7 | Experimental setup to study the interaction of particles and filter medium with varying angle of attack α . **A** Small circular flow tank with a pump, honeycombs before and after the test section, and a holder for the filter medium. **B** The holder consists of a plate with a rotating disc, featuring 10° increments, and a frame that holds the filter media with mesh sizes of 53, 100, and $300\ \mu\text{m}$, allowing the passage of fluid through these mesh sizes. Four particle types were tested: **C** brine shrimp eggs, **D** brine shrimp adults, **E** MP fragments, and **F** MP fibres (for particle specifications, see Table 2). Scale = 1 mm.



vary dynamically over time, complex 3D vortices may occur, especially with the swirl and snail inlet, and the fluid may contain particles or exhibit non-uniform properties. These factors can influence local flow patterns, filtration efficiency and fouling behaviour, which could be subject of future CFD analysis of the FiF.

In the future, the cleaning process will be one of the major challenges to improve the FiF. Cleaning includes the reduction of the fluid volume in the concentrate, drying and disposal of retained MPs and dirt. Therefore, it could be beneficial to further analyse the inherent cleaning process in fishes such as whale sharks, which use back-flushing⁴³. Another advancement would be a sensory system that couples the cleaning intervals to the pressure difference across the filter medium. As more fibres will accumulate in the filter element, the pressure difference will increase. Automatic cleaning at a specific pressure threshold could prevent clogging and inform the user when manual cleaning or replacement is required. Additionally, the FiF will have to be tested with mixed particles, a higher particle load to determine the dirt-holding capacity before clogging and failure, and other particle types, especially those that are present in washing machine effluents, like textile fibres from natural sources, oils, sand, dust, pollen and hair and detergents^{13,44}. It is estimated that washing machine filters must work in the presence of around 30 g of potential solids when using powder detergents and around 10 g when using liquid or gel detergents⁴⁴. These quantities are relevant for the size of the filter, its 'dirt-holding' capacity and cleaning intervals³¹.

When biological models are investigated, functional constraints need to be considered. For example, the gill arch system serves as the filter medium for retaining food particles, while also being involved in gas exchange and ensuring a constant flow along the gill filaments. This poses a trade-off, which might limit the performance of both traits⁴⁵. For solid-liquid separation, Hamann and Blanke⁴⁶ identified 35 different particle separation mechanisms in suspension-feeders⁴⁶. Even within ram-feeding fishes—a single category among those mechanisms—a following study found three morphotypes just within five species¹⁹. This variation demonstrates the significant potential for developing bio-inspired filters and further optimising the FiF. For example, the filter elements could be more tailored towards a single morphotype based on characterised traits. The angle of attack could vary from anterior to posterior, as seen in the Atlantic mackerel, or the radial geometry could be modified to more closely mimic the upward-bending gill arches of the Atlantic pilchard and Atlantic herring¹⁹. Notably, biomimetic research is not only a means of technological innovation, it also contributes to a deeper understanding of the biological models themselves. As demonstrated in the angle-of-attack experiments (Fig. 1), particle shape influences rolling behaviour and deposition, a factor often overlooked in models that assume spherical particles²⁶. For instance, the behaviour of adult brine shrimp in contact with the filter was less

consistent than that of other particle types (Fig. 1D). At low angles, post-contact velocity occasionally exceeded pre-contact velocity (Supplementary Fig. 3B), suggesting a possible repulsion response⁴⁷. Such findings are both relevant to interpret the adaptations in biological models and optimisation of engineered filters to certain particle types.

Methods

To design and validate a self-cleaning FiF for microplastic retention, we conducted a series of design, flow and performance tests.

Angle of attack and particle retention experiments

The working principle of the filter is based on the semi-cross flow filtration described in our previous study on the feeding morphology in ram-feeding fishes¹⁹. In models for particle deposition in cross-flow filtration, it was found that the probability of particle rolling increases with increasing lateral crossflow velocity parallel to the filter medium and vice versa²⁶. Similarly, we hypothesise that a decrease in the angle of attack increases the chance of particle rolling. At higher angles, the crossflow velocity is less parallel to the filter medium and the force in direction of the permeate increases, which increases the change of particle deposition. In order to test the influence of α on particle retention, an experimental setup was designed in which a filter medium can be positioned at angles from 0° (parallel) to 90° (perpendicular) in increments of 10° towards the unidirectional flow in a small, circular water tunnel (Fig. 7A, B). Only angles from 10° to 60° were studied because this is the range measured in the micro-CT scans of the gill arch system of the fish (Supplementary Fig. 2). Three filter media with a mesh size of $53\ \mu\text{m}$ (open area 40%, PES 53/40, Saati S.p.A, Italy), $100\ \mu\text{m}$ (open area 44%, PA6.6-100/51-44, Bückmann GmbH & Co. KG, Germany), and $300\ \mu\text{m}$ (open area 45%, 300/45/FDA, Franz Eckert GmbH) were selected, and four types of particles were tested: brine shrimp eggs ($0.242 \pm 0.019\ \text{mm}$) and adults ($6.112 \pm 0.993\ \text{mm}$) to represent natural food sources, and MP fragments (Polyamide, median diameter $130\ \mu\text{m}$,) and MP fibres (Polyamide, 2 mm length) to represent different MPs (Fig. 7C–F and Table 2). The flow velocity was set to around 11 cm/s, which is in a similar range of flow velocities in washing machine outlet pipes with $<0.5\ \text{m/s}$ and particle velocities inside fish mouths during filter feeding with $0.2\text{--}0.65\ \text{m/s}$ ¹⁹. A camera (Nikon D850, Macro lens Nikkor AF-S 24-120 mm 1:4 G ED) was positioned outside the tank to film the particle encounter on the filter medium. After each rotation, the camera's focal plane was adjusted, and the scale was recorded by filming a ruler close to the filter medium. The videos of the brine shrimp eggs, adults, and MP fibres were analysed manually with ImageJ (Version 2.3.0) and the manual tracking plugin. A fixed point was selected on the particles to track their motion. Each particle that came in contact with the mesh was tracked when it entered the recorded video section and ended when it was out of frame. The frame in which the particles

Table 2 | Overview of the five different test particles and fibres used for the experiments in this study

Particles	Length [mm]	Material	Density	Additional information	Source/fabrication
Brine shrimp eggs	0.242 ± 0.019	NA	1.09 g/cm ³	-	University of Bonn
Brine shrimp adults	6.112 ± 0.993	NA	1.09 g/cm ³	-	Breeding by Sea Life Oberhausen
Cotton fibres	0.2–4	Cotton, white	1.51 g/cm ³	DMT Prüfstaub Typ 8	Provided by Hengst SE
Polyamide fragments (MP fragments)	0.00002–2	Polyamide, orange	1.08 g/cm ³	^a see manufacturing process	VESTAMID® LX9057 orange E20081 by Evonik
Flock fibres (MP fibres)	2 mm (dtex 3.3)	Polyamide, green	1.08 g/cm ³	Dtex = 22	Borchert + Moller GmbH & Co. KG

^aThe orange polyamide polymer (VESTAMID® LX9057 orange E20081) was selected because its density is close to water and its bright colour to be able to observe the particles during the experiments. The polymer came in pellets and was reduced in size through a cryogenic grinding process at Fraunhofer UMSICHT, Oberhausen. The particle size distribution in the obtained powder was characterised by a Malvern Mastersizer 2000 (Hydro2000S). Particle size ranges between 0.020 and 2000 with a median of around 130 µm.

touched the mesh was noted as ‘contact’. Before further analyses, the number of frames was reduced to a maximum of 20 frames before and after the contact frame. The MP fragments were semi-automatically analysed. Therefore, only the frame of contact and the position of the MP fragment within the frame were noted. Afterwards, Python (Python Software Foundation) was used to automatically track the pre-identified particles and extract the particle velocity in each frame to a maximum of 20 frames before and after the contact frame.

Based on the extracted particle velocity in a maximum of 40 frames for all four particle types, a Boltzmann sigmoidal curve⁴⁸ was fitted to the data using Python (Python Software Foundation). Based on the fit, the average velocity before contact, average velocity after contact, and R^2 of the fit were extracted for further analysis in the R programming environment (R Core Team, R version 4.2.2, 2022). The mean of R^2 was calculated to compare the quality of the fits of each particle type and describe the steadiness of particle motion (see Supplementary Fig. 3A for examples). A threshold value was set to 0.3 cm/s (20% of the average minimum velocity of all observed particles after contact with the filter medium) to distinguish rolling particles (>0.3 cm/s) and particles that stopped on the filter medium (<0.3 cm/s). The ratio of the number of rolling particles to all particles gives the probability of rolling for each α , mesh size, and particle type. Polynomial regression was fitted to the data to describe the influence of α on probability of rolling. Because only six points are available for the fit, linear to cubic polynomial regression (degree 1–3) was applied to prevent an over-fitted high-polynomial regression. The Akaike’s Information Criterion (AIC) was used to identify the best fit⁴⁹.

Biological models and filter design

The technical requirements of washing machines were matched with the suspension feeding mechanisms (SFMs) (Supplementary Note 1) of suspension feeders reviewed in a previous publication⁴⁶ to identify analogous traits in biological models. The geometry should be flat or funnel-shaped in a pipe, the desired retained particle size should be 100 µm–10 mm, the driving force should be passive, pumping, or forward movement, and SFMs should work with a water velocity of >1 cm/s. Ram-feeding fish meet all those criteria. As proposed by Hamann et al.¹⁹, we define the filtration process with $0^\circ < \alpha < 90^\circ$ as semi-cross-flow filtration¹⁹. Similar to cross-flow filtration, the particles in semi-cross-flow filtration can either be retained on the surface of the filter medium as retentate (M_R), collected in the concentrate (M_C), or pass the filter medium and end up in the permeate (M_P). The volume flow is diverted into the clean permeate (V_P) and particle-loaded concentrate (V_C) (Fig. 3A).

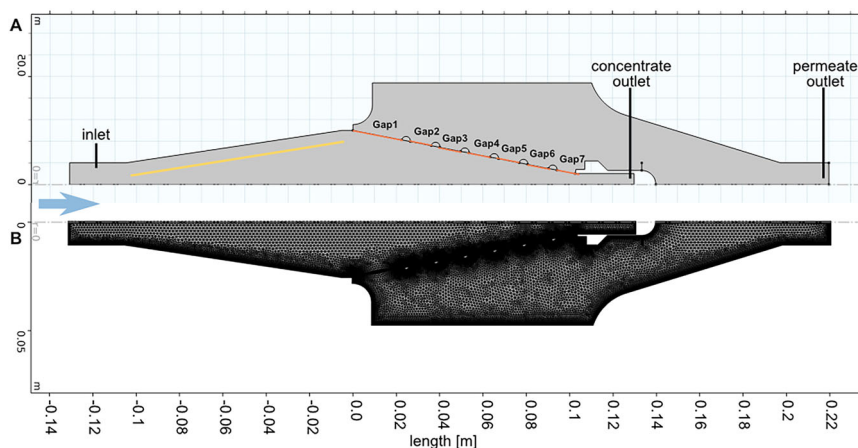
The basic shape of the filter element is a cone. The base of the cone is the fish mouth opening and was set to a diameter of 50 mm. The apex of the cone was designed as the concentrate outlet to resemble the oesophagus and has a diameter of 10 mm (Fig. 2A and Table 1). Depending on the filter element size, four to six curved struts, resembling the appearance of the GA, were implemented to support the filter mesh. The support structures of the filter element were 3D-printed (PolyJet multi-material 3D Printer, StrataSys J35TM Pro) with a

Polyacrylate polymer resin (VeroUltra, StrataSys). The off-the-shelf filter mesh forms square meshes and mimics GR and denticles (Fig. 2). Across all FiF experiments, we used three different mesh sizes, i.e. 53 µm (open area 40%, PES 53/40, Saati S.p.A, Italy), 78 µm (open area 50%, PES 78/50, Saati S.p.A, Italy) and 100 µm (open area 44%, PA6.6-100/51-44, Bückmann GmbH & Co.KG, Germany). This is within the range of mesh sizes calculated for the ram-feeding fish, which ranges from 0.007 to 0.148 mm² for the mesh sizes with an open area of 51.8–71.4%¹⁹, and as recommended in studies to retain MPs fibres in washing machines^{40,50}. The filter mesh was glued inside the support structures using acrylic super glue.

The hyoid bone, the short GR, denticles, and teeth form a structured surface in the two scombrid species (Fig. 2C). The function of these structures is not clear yet, but the hair and denticles might capture particles. Alternatively, we assume that the surface structures could create additional turbulence to keep the filter medium clean, similar to the d-type structure found in the American Paddlefish²² or dynamic cross-flow filtration⁵¹. In order to observe the influence of surface structures and study their effect on the filter performance, a line with ellipsoids was designed, 3D-printed (PolyJet multi-material 3D Printer, StrataSys J35TM Pro), and glued onto the first half of the lengthways support structures of the filtering element to mimic the short GR and hyoid bone in the scombrid species (Fig. 2C). The teeth and denticles were mimicked by hooked tape (VELCRO® HTH820) consisting of rows with hooks facing opposite directions. In one filter element, the hooked tape was glued in the posterior half of the filter, and in another, it was glued on the entire length (Fig. 2C).

The filter housing is modular and consists of an inlet, a flange, a transparent pipe, and an outlet (Fig. 3). The inlet leads the suspension towards the filter element. The brass flange connects the inlet, transparent pipe, and outlet with four stainless steel screws. A small screw in the flange to release air from the filter housing. The transparent pipe allows us to observe the filtration process in and around the filter element and comes in two sizes to test different filter element lengths. The outlet features two separate outputs for concentrate and permeate, which are connected to pipes and containers. Due to the unique design of the inlet, flange, and outlet sections, they had to be custom-made. The flange was manufactured in the workshop at the University of Bonn. The inlet and outlet were 3D-printed (PolyJet multi-material 3D Printer, StrataSys J35TM Pro) using a waterproof acrylate resin polymer (VeroUltra, StrataSys). Two automatic valves at each of the outlet pipes control the outflow and mimic the cleaning behaviour of the fish (for the development of the test setup, see Supplementary Note 2). The valve at the permeate outflow was normally open (EPK-1502-NO, 24 V, Takasago, BMT Fluid Control Solutions GmbH), and the valve at the concentrate outflow was normally closed (EPK-1502-NC, 24 V, Takasago, BMT Fluid Control Solutions GmbH). Both valves were connected in parallel and adjustable with a custom-made control unit. During cleaning, the valve at the concentrate opens, and the valve at the permeate closes simultaneously. The cleaning interval can be set to durations between 13 and 86 s, and the cleaning process itself can be set to 0.6–6.5 s.

Fig. 8 | Virtual setup for the computational fluid dynamics (CFD) study of the FiF. A The 2D geometry was based on a FiF with the Large-11 filter element and the long inlet tapered at 9°. The inlet was modelled with and without inner wall (indicated by yellow line). The cross section of the filter element led to seven gaps between the support structures (Gap 1–Gap 7). The filter mesh at the gaps was modelled with the COMSOL® inbuilt screen function (indicated by dashed orange lines). The direction of the flow is indicated by the blue arrow. **B** The free tetrahedral mesh is extra fine at the filter element and has two boundary mesh layers on all solid surfaces.



Computational fluid dynamics of filter element

We performed CFD to investigate the stationary flow behaviour in the FiF using COMSOL Multiphysics® (Version 6.3) and the CFD Module. The 2D geometry is half of the cross-section of the FiF with the Large 11 filter element (Fig. 8A). At the inlet, a constant normal inflow velocity of 0.05 m/s was applied. The inlet diameter is 0.02 m, resulting in a Reynolds number below 1000 for water at 10 °C, which justifies the assumption of laminar flow (with a water density of 999.7 kg/m³ and a dynamic viscosity of 0.001308 kg/m·s). The simulation assumes incompressible, laminar flow solving the Navier-Stokes equations and a pressure boundary condition ($p = 0$) was applied at the outlets (permeate and concentrate). The filter element consists of seven separate gaps (Gap 1–Gap 7) between the gill arch like support structures (Fig. 8A). Each gap was modelled as a ‘Screen’ boundary condition in COMSOL®, with a solidity σ (blocked area/total area) of 0.56 (Screen Type: Square mesh), which is similar to the open area of the filter media used in the physical experiments. The solidity σ is calculated from the resistance coefficient K ($K = 0.98((1 - \sigma_s)^{-2} - 1)$ ^{1,09} and the refraction coefficient η ($\eta = \sqrt{\frac{K^2}{2} + 1} - (K/4)$)⁵². The domain was discretized using a free tetrahedral mesh with two boundary mesh layers on all solid surfaces (Fig. 8B). We found no dependence of the solution (flow velocity vectors at the mesh) on the mesh in the range from 18,000 domain elements and 1100 boundary elements up to 140,000 domain elements and 3800 boundary elements. The final mesh consisted of approximately 42,000 elements with a maximum element size of 1.65 mm in the main domain, and refined elements of 0.12 mm near boundaries (Fig. 8B). Convergence criteria as well as monitoring the solution variables of the model was automatically ensured by the COMSOL® software using the default settings of the CFD module⁵². The simulation aims to qualitatively analyse the flow field, with a particular focus on the effective angle of attack $\alpha(\text{eff})$. This angle was measured in COMSOL® between the filter mesh and the flow vectors of the individual streamlines relative to the filter mesh. We tested the influence of three different operational modes if the filter house: (1) permeate outlet open and concentrate outlet closed (filtration mode), (2) concentrate outlet open and the permeate outlet open (single cleaning mode), and (3) concentrate outlet open and the permeate outlet closed (double cleaning mode). Additionally, we tested the influence of an additional inner wall inside the long inlet at 9° to further observe the effect on $\alpha(\text{eff})$ along the filter element. The angle $\alpha(\text{eff})$ along the filter element was exported as an excel file and plotted over the length of the filter element using the R Programming Environment (R Core Team, R version 4.2.2, 2022).

Filtration efficiency testing

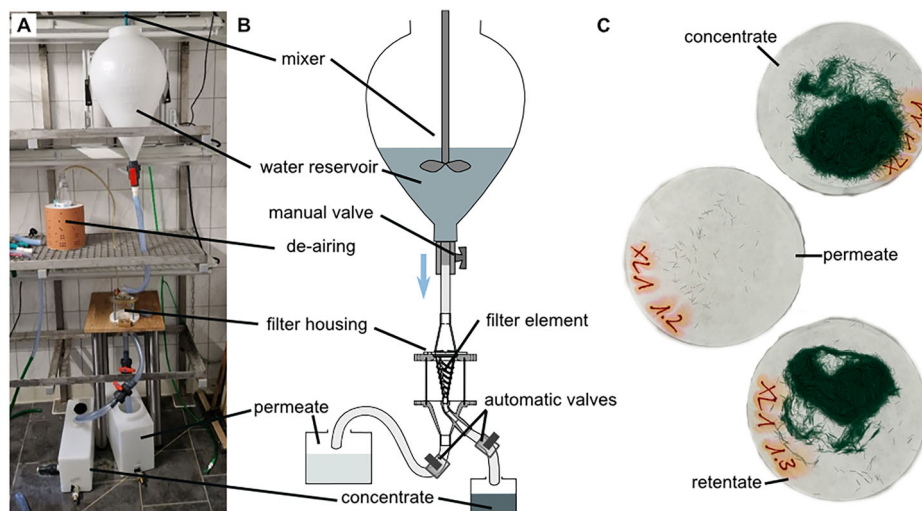
A test stand was built to test the FiF’s volume flow and particle filtration efficiency. The basic setup consists of a water reservoir (FastBrewing Starter Kid, 30 L Volume) with a mixer, a pipe that leads the feed (V_F , M_F) towards the FiF, a pipe for the concentrate, a pipe for the permeate, and two

containers to collect both fractions (Figs. 9A, B and 3A). The simple setup reduces dust and dirt from influencing mass fraction measurements (Supplementary Notes 2 and 3) and has steady flow conditions. The volume flow will naturally decrease due to the decrease of hydrostatic pressure. Preliminary experiments were performed to test, optimise and measure volume flow through the test stand (Supplementary Note 2). During these experiments, we observed that cotton fibres would lead to a higher chance of clogging and that the MP fragments had a very low recovery ratio. We observed that MP fragments adhered to the inner surface of the reservoir, which could be one reason for the low recovery ratio. Therefore, we proceeded with MP fibres only and added liquid detergent to increase MP fibre suspension, which had no influence on the analytical procedure (Supplementary Note 3).

In a first set of experiments, the Large-11 filter element was compared to the dead-end filter element (DE) with the same filtration area (Table 1). The dead-end filter element has a cylindrical shape with a α of 0°, which resembles the cartridge filter design of a commercial washing machine filter (Fig. 5C). It is closed at the end, so the retentate cannot be removed through the concentrate outflow during filtration. Both were equipped with a commercial filter medium from Polyamide 6.6 with a mesh size of 100 μm and an open area ratio of 44% (Bückmann PA6.6-100/51-44). The filter mesh is temperature-resistant up to 140–180 °C and stable in soapy water. To test the influence of surface structures as observed in ram-feeding mackerels in previous studies by the authors, the same Large-11 filter elements were equipped with hooked tape 50% of the length of the support structures (L-50), 100% of the support structures (L-100) and with 3D printed bumps of 50% of the support structures (L-B) (Fig. 2). Before each trial, the valves were closed, the FiF was filled with clean water and de-aired, and 0.625 g of MP fibres, 5 ml of liquid detergent were mixed in 25 l of clean water in the water reservoir. The valve in the permeate pipe was opened to start the experiment. Cleaning was automatically set when 10 and 20 l passed the FiF. After the second cleaning when the valves were closed again, the experiment was stopped. The test stand and FiF were rinsed with clean water between each trial. The order of the experiments was chosen at random and each test condition was replicated five times ($n = 5$).

In a second set of experiments, several factors were changed to investigate their effects filtration performance for the application in washing machines (Supplementary Note 1). To test the FiF’s performance and understand the effects, only one factor was changed at a time. Overall, we tested the influence of three different filter element length with $\alpha = 11^\circ$ (Small-11, Medium-11, Large-11, Table 1), of α in the small filter element with $\alpha = 11^\circ$ and $\alpha = 22^\circ$ (Small-11, Small-22), of three different inlets (long, snail and swirl), and of three different mesh sizes with 53, 78 and 100 μm in the Large-11 and with 53 and 100 μm in the Small-11 filter element. Before each trial, the valves were closed, the FiF was filled with clean water and de-aired, and 0.5 g of MP fibres, 5 ml of liquid detergent were mixed in 20 l of

Fig. 9 | Design of the test stand to measure filter performance. **A** The test stand consists of a water reservoir with a mixer, the filter housing with a de-airing option, and two containers to collect the permeate and concentrate. **B** The filter housing allows for testing of different filter elements. A manual valve enables regulating the inflow, and two automatic valves regulate the outflow and cleaning of the filter element. **C** After each experiment, three MP fibre fractions (green) were analysed: MP fibres collected in the concentrate (top), MP fibres collected in the permeate (middle), and MP fibres retained in the filter element, the retentate (bottom). For details of the test procedure, see Supplementary Notes 2 and 3.



clean water in the water reservoir. The valve in the permeate pipe was opened to start the experiment. Cleaning was automatically set when 5 and 10 l passed the FiF. Note that the second set of experiments used a smaller feed volume. After the second cleaning, when the valves were closed again, the experiment was stopped. The test stand and FiF were rinsed with clean water between each trial. The order of the experiments was chosen randomly, and a total of five trials per combination were tested.

Three fluid volume (V) and mass (M) samples were taken after each trial: (1) the total volume of the concentrate (V_C and M_C), (2) one liter of the permeate (V_P and M_P), and (3) all the MP fibres that remained within the filter, i.e. the retentate (M_R) re-suspended in a maximum of one liter. The MP fibre mass fractions were separated from the water using a suction filter (Nalgene Reusable Bottle Top Filter) with round filtering papers (ROTI-LABO Type 11 A, ϕ 45 mm, retention range 12–15 μm) and a vacuum pump (Vaccubrand MZ 2 C, 1.7 $\text{m}^3/\text{h} = 28.3$ l/min). Prior to the vacuum filtration, the filtering papers were labelled, dried in a heating cabinet (minimum 30 min), cooled down in a desiccator (minimum 30 min), and weighted with a precision scale (Sartorius ED153-CW, weighing capacity 150 g, readability 0,001 g, repeatability (std. deviation) ± 0.001 g). After the samples were poured onto the suction filter, the bottle, bottle cap, and walls of the suction filter were rinsed with deionized water, so all MP fibres were collected on the filtering paper. Afterwards, the filtering papers with the MP fibres (Fig. 9C) were dried in a heating cabinet and a desiccator and weighed again. The weight difference determined the fibre mass fraction of each sample. The samples of the permeate were thereby multiplied by the total filtered volume minus the volume in the concentrate to account for the subsample taken from the total permeate volume.

Contamination controls

To test the lab contamination and the scale's accuracy, three control samples of 1000 ml of clean tap water were analysed using the same analytical procedure and weighed three times. The weight difference of the filter papers without experimental samples are 0.00107, 0.00010, and 0.00010 g. Additionally, we ran three blank trials after rinsing the test stand and without adding MP fibres to determine the contamination of the test stand and the influence of previous trials. The weight difference of the filter papers with the blank samples are 0.00082, -0.00029 and -0.00059 g for the concentrate samples and -0.00667 , -0.01148 and -0.01574 g for the permeate samples. Due to these differences in the permeate samples, all results are rounded to two decimal places. Additionally, when the weight difference of permeate samples were negative (difference of filter paper before and after experiments) but within ± 0.01 g, they were changed to 0.00 g as we assume that contamination had an influence. We changed a total of nine negative values to 0.00.

Performance metrics

The different FiF combinations were evaluated based on a set of established filtration performance metrics. The main goal of solid-liquid filters is to separate solid particles from a fluid and is usually expressed as the filtration efficiency. The filtration efficiency is the ratio of upstream particle concentration to the downstream particle concentration of the filter medium and is expressed in per cent³¹.

We calculated two filtration efficiencies to account for the three different MP fibre mass fractions of the FiF. E_R is the share of MP fibres that are retained in the filtration system, i.e. the concentrate and retentate (Eq. 1), which can also be expressed as the subtraction of the share found in the permeate and is a typical performance criterion for filters, also for filters in washing machines⁴⁰. If all particles were retained within the filter and none were lost to the permeate, E_R would be 100%.

$$E_R = \left(\frac{M_C + M_R}{M_{C+P+R}} \right) * 100 = \left(1 - \left(\frac{M_P}{M_{C+P+R}} \right) \right) * 100 \quad (1)$$

with E_R = Filtration efficiency in concentrate and retentate, M_C = Particle mass in concentrate [g], M_P = Particle mass in permeate [g], M_R = Particle mass in retentate [g].

The other filtration efficiency parameter is E_C , which is the share of MP fibres that is retained in the concentrate (Eq. 2). E_C should be as high as possible because the FiF is designed to accumulate most of the MP fibres in the concentrate to avoid clogging.

$$E_C = \left(\frac{M_C}{M_{C+P+R}} \right) * 100 \quad (2)$$

E_C = Filtration efficiency in concentrate, M_C = Particle mass in concentrate [g], M_P = Particle mass in permeate [g], M_R = Particle mass in retentate [g].

The concentrating factor X is the ratio of the feed volume in the water reservoir to the fluid volume collected in the concentrate (Eq. 3). The aim is to keep the concentrating factor as high as possible so that post-filtration treatment of the concentrate is kept minimal.

$$X = \left(\frac{V_F}{V_C} \right) \quad (3)$$

with X = Concentrating factor, V_F = Feed volume [l], V_C = Concentrate volume [l].

Because the FiF is similar to a cross-flow filter, the performance is also described as the yield in concentrate η_C . This parameter combines the MP fibre mass in the concentrate E_R and the concentrating factor X as is

expressed in percent (Eq. 4). The function is nonlinear and increases sharply as E_R approaches 100%. A high value indicates a good-performing cross-flow filter.

$$\eta_C = X^{(E_R-100)} * 100 \quad (4)$$

with η_C = Yield in concentrate [%], X = Concentrating factor, E_R = Filtration efficiency.

The volume flow rate was determined as part of the preliminary experiments and is described in the Supplementary Material (Supplementary Note 2 and Supplementary Fig. 5).

All data were analysed in the R Programming Environment (R Core Team, R version 4.2.2, 2022) and visualised using the ggplot2 package⁵³. We report mean values with standard deviation in the text. The experimental studies conducted served to elucidate the filter mechanism. More and differently designed experimental data would be needed for a comprehensive statistical analysis. The available data for the filter performance were therefore primarily evaluated qualitatively. All figures were laid out with Scribus (Version 1.5.8).

Data availability

All data is available in the main text or the supplementary materials.

Received: 7 July 2025; Accepted: 20 October 2025;

Published online: 05 December 2025

References

1. Triebekom, R. et al. Relevance of nano- and microplastics for freshwater ecosystems: a critical review. *TrAC* **110**, 375–392 (2019).
2. Chia, R. W., Lee, J. Y., Kim, H. & Jang, J. Microplastic pollution in soil and groundwater: a review. *Environ. Chem. Lett.* **19**, 4211–4224 (2021).
3. Evangelidou, N. et al. Atmospheric transport is a major pathway of microplastics to remote regions. *Nat. Commun.* **11**, 3381 (2020).
4. Gkoutselis, G. et al. Microplastics accumulate fungal pathogens in terrestrial ecosystems. *Sci. Rep.* **11**, 1–13 (2021).
5. Yin, L. et al. Interactions between microplastics/nanoplastics and vascular plants. *Environ. Pollut.* **290**, 117999 (2021).
6. Nelms, S. E., Galloway, T. S., Godley, B. J., Jarvis, D. S. & Lindeque, P. K. Investigating microplastic trophic transfer in marine top predators. *Environ. Pollut.* **238**, 999–1007 (2018).
7. Zhao, B. et al. Science of the total environment the potential toxicity of microplastics on human health. *Sci. Total Environ.* **912**, 168946 (2024).
8. Rochman, C. M. et al. Rethinking microplastics as a diverse contaminant suite. *Environ. Toxicol. Chem.* **38**, 703–711 (2019).
9. Steensgaard, I. M. et al. From macro- to microplastics - Analysis of EU regulation along the life cycle of plastic bags. *Environ. Pollut.* **224**, 289–299 (2017).
10. Munhoz, D. R., Harkes, P., Beriot, N., Larreta, J. & Basurko, O. C. Microplastics: a review of policies and responses. *Microplastics* **2**, 1–26 (2022).
11. Auta, H. S., Emenike, C. U. & Fauziah, S. H. Distribution and importance of microplastics in the marine environment: a review of the sources, fate, effects, and potential solutions. *Environ. Int.* **102**, 165–176 (2017).
12. Clausen, L. P. W., Hansen, O. F. H., Oturai, N. B., Syberg, K. & Hansen, S. F. Stakeholder analysis with regard to a recent European restriction proposal on microplastics. *PLoS ONE* **15**, e0235062 (2020).
13. Zhang, Y.-Q. et al. Microplastics from textile origin – emission and reduction measures. *Green Chem.* **23**, 5247–5271 (2021).
14. Boucher, J. & Friot, D. *Primary Microplastics in the Oceans: A Global Evaluation of Sources*. <https://www.iucn.org/content/primary-microplastics-oceans> (2017).
15. Sherrington, C., Darrah, C., Hann, S., Cole, G. & Corbin, M. Study to support the development of measures to combat a range of marine litter sources. Report for European Commission DG Environment. **429**, 1–432 (2016).
16. Masselter, T. et al. Improvement of a microfiber filter for domestic washing machines. *Bioinspir. Biomim.* **18**, 016017 (2023).
17. Iyare, P. U., Ouki, S. K. & Bond, T. Microplastics removal in wastewater treatment plants: a critical review. *Environ. Sci. Process. Impacts* **6**, 2664–2675 (2020).
18. Gao, D., Li, X. & Liu, H. Source, occurrence, migration and potential environmental risk of microplastics in sewage sludge and during sludge amendment to soil. *Sci. Total Environ.* **742**, 140355 (2020).
19. Hamann, L. et al. Diversity of filter feeding and variations in cross-flow filtration of five ram-feeding fish species. *Front. Mar. Sci.* **10**, 1–21 (2023).
20. Sanderson, S. L. L., Cheer, A. Y. A. Y., Goodrich, J. S. J. S., Graziano, J. D. J. D. & Callan, W. T. T. Crossflow filtration in suspension-feeding fishes. *Nature* **412**, 439–441 (2001).
21. Sanderson, S. L. et al. Mucus entrapment of particles by a suspension-feeding tilapia (Pisces: Cichlidae). *J. Exp. Biol.* **199**, 1743–1756 (1996).
22. Brooks, H., Haines, G. E., Lin, M. C. & Sanderson, S. L. Physical modeling of vortical cross-step flow in the American paddlefish, *Polyodon spathula*. *PLoS ONE* **13**, e0193874 (2018).
23. Sanderson, S. L., Roberts, E., Lineburg, J. & Brooks, H. Fish mouths as engineering structures for vortical cross-step filtration. *Nat. Commun.* **7**, 11092 (2016).
24. Storm, T. J., Nolan, K. E., Roberts, E. M. & Sanderson, S. L. Oropharyngeal morphology related to filtration mechanisms in suspension-feeding American shad (Clupeidae). *J. Exp. Zool. Part A Ecol. Integr. Physiol.* **333**, 493–510 (2020).
25. Paig-Tran, E. W. M. W. M., Bizzarro, J. J. J. J., Strother, J. A. J. A. & Summers, A. P. A. P. Bottles as models: predicting the effects of varying swimming speed and morphology on size selectivity and filtering efficiency in fishes. *J. Exp. Biol.* **214**, 1643–1654 (2011).
26. Di, H., Martin, G. J. O. & Dunstan, D. E. Characterization of particle deposition during crossflow filtration as influenced by permeate flux and crossflow velocity using a microfluidic filtration system. *Front. Chem. Sci. Eng.* **15**, 552–561 (2021).
27. Richardsons, J. F., Harker, J. H. & Backhurst, J. R. *Coulson and Richardson's Chemical Engineering: Particle Technology and Separation Processes* Vol. 2 (Butterworth-Heinemann, 2002).
28. Scholz, W. & Lucas, M. Techno-economic evaluation of membrane filtration for the recovery and re-use of tanning chemicals. *Water Res.* **37**, 1859–1867 (2003).
29. Kowalska, I., Kabsch-Korbutowicz, M., Majewska-Nowak, K. & Pietraszek, M. Removal of detergents from industrial wastewater in ultrafiltration process. *Environ. Prot. Eng.* **31**, 207–219 (2005).
30. Żyła, R., Foszpańczyk, M., Olak-Kucharczyk, M., Marszałek, J. & Ledakowicz, S. Removal of organic compounds with an amino group during the nanofiltration process. *Membranes* **12**, 1–14 (2022).
31. Sutherland, K. *Filters and Filtration Handbook* (Elsevier, 2008).
32. Piedrahita, R. H. & Hung, T. C. Crossflow filtration particle separator. The Patent number is US 2015/0143784 A1. The Regents of the University of California USA (2015).
33. Hung, T. & Piedrahita, R. H. Experimental validation of a novel bio-inspired particle separator. *Aquac. Eng.* **58**, 11–19 (2014).
34. Divi, R. V., Strother, J. A. & Paig-Tran, E. W. M. Manta rays feed using ricochet separation, a novel nonclogging filtration mechanism. *Sci. Adv.* **4**, eaat9533 (2018).
35. Li, Z., Tan, C. M., Tio, W., Ang, J. & Sun, D. D. Manta ray gill inspired radially distributed nanofibrous membrane for efficient and continuous oil–water separation. *Environ. Sci. Nano* **5**, 1466–1472 (2018).
36. Zhang, X. et al. Biomimetic gill-inspired membranes with direct-through micropores for water remediation by efficiently removing microplastic particles. *Chem. Eng. J.* **434**, 134758 (2022).

37. Tsai, C., Hwu, C. & Wei, Y. Biomimetic fuel filtration for air vehicles based on Ricochet separation inspired by manta rays. *Sep. Purif. Technol.* **371**, 133331 (2025).
 38. Schroeder, A., Marshall, L., Trease, B., Becker, A. & Sanderson, S. L. L. Development of helical, fish-inspired cross-step filter for collecting harmful algae. *Bioinspir. Biomim.* **14**, 056008 (2019).
 39. Ramasamy, R., Nallendiran, L. & Subramanian, R. B. Microfiber filters for laundry: a systematic review of effectiveness and future research directions for pollution mitigation. *Water Air Soil Pollut.* **236**, 1–24 (2025).
 40. Browne, M. A., Ros, M. & Johnston, E. L. Pore-size and polymer affect the ability of filters for washing-machines to reduce domestic emissions of fibres to sewage. 1–17 <https://doi.org/10.1371/journal.pone.0234248> (2020).
 41. McIlwraith, H. K. et al. Capturing microfibers – marketed technologies reduce microfiber emissions from washing machines. *Mar. Pollut. Bull.* **139**, 40–45 (2019).
 42. Hernandez, E., Nowack, B. & Mitrano, D. M. Polyester textiles as a source of microplastics from households: a mechanistic study to understand microfiber release during washing. *Environ. Sci. Technol.* **51**, 7036–7046 (2017).
 43. Motta, P. J. et al. Feeding anatomy, filter-feeding rate, and diet of whale sharks *Rhincodon typus* during surface ram filter feeding off the Yucatan Peninsula, Mexico. *Zoology* **113**, 199–212 (2010).
 44. Schöpel, B. & Stamminger, R. A comprehensive literature study on microfibres from washing machines. *Tenside Surfactants Deterg.* **56**, 94–104 (2019).
 45. Broeckhoven, C. & du Plessis, A. Escaping the labyrinth of bioinspiration: biodiversity as key to successful product innovation. *Adv. Funct. Mater.* **2110235**, 1–8 (2022).
 46. Hamann, L. & Blanke, A. Suspension feeders: diversity, principles of particle separation and biomimetic potential. *J. R. Soc. Interface* **19**, 20210741 (2022).
 47. Rashid, M. T. et al. Artemia swarm dynamics and path tracking. 555–563 <https://doi.org/10.1007/s11071-011-0237-6> (2012).
 48. Motulsky, H. & Christopoulos, A. *Fitting Models to Biological Data using Linear and Nonlinear Regression*. (GraphPad Software Inc., 2003).
 49. Burnham, K. P. & Anderson, D. R. *Model Selection and Multimodel Inference: A Practical Information-Theoretic Approach*. (Springer New York, 2002).
 50. De Falco, F. et al. Development and performance evaluation of a filtration system for washing machines to reduce microfiber release in wastewater. *Water Air Soil Pollut.* **232**, 406 (2021).
 51. Bott, R., Langeloh, T. & Ehrfeld, E. Dynamic cross flow filtration. *Chem. Eng. J.* **80**, 245–249 (2000).
 52. COMSOL Multiphysics®. CFD Module User's Guide. 710 at (2024).
 53. Wickham, H. *ggplot2: Elegant Graphics for Data Analysis*. (Springer International Publishing, 2016).
- experience of testing microplastic filters in a lab environment. LH and AB were supported by the European Research Council (ERC) under the European Union's Horizon 2020 research and innovation program (grant agreement no. 754290). CR, HH, KS and CG were supported by the Federal Ministry of Education and Research (BMBF) under the program "Ideenwettbewerb Biologisierung der Technik" (grant agreement no. 13XP5164A) awarded to A.B. and Dr. Gehrke.

Author contributions

L.H., A.B., H.H., C.G. and C.R. planned and conceptualised the study. L.H., H.H., C.R. and C.G. developed the methodology. L.H., K.S., H.H. and C.R. performed and analysed the physical experiments. CG and HH performed and analysed the numerical experiments. L.H., H.H., C.R. and C.G. visualised the data and L.H. prepared all final figures. L.H. and A.B. performed project supervision. L.H. wrote the main manuscript text. All authors reviewed and edited the manuscript.

Competing interests

A patent for the new fish-inspired filter was filed at the German Patent and Trade Mark Office in March 2023 (Germany: DE102023001223A1 granted, World: WO002024199585A1 pending). Otherwise, the authors declare that they have no competing interests.

Additional information

Supplementary information The online version contains supplementary material available at <https://doi.org/10.1038/s44454-025-00020-2>.

Correspondence and requests for materials should be addressed to Leandra Hamann.

Reprints and permissions information is available at <http://www.nature.com/reprints>

Publisher's note Springer Nature remains neutral with regard to jurisdictional claims in published maps and institutional affiliations.

Open Access This article is licensed under a Creative Commons Attribution 4.0 International License, which permits use, sharing, adaptation, distribution and reproduction in any medium or format, as long as you give appropriate credit to the original author(s) and the source, provide a link to the Creative Commons licence, and indicate if changes were made. The images or other third party material in this article are included in the article's Creative Commons licence, unless indicated otherwise in a credit line to the material. If material is not included in the article's Creative Commons licence and your intended use is not permitted by statutory regulation or exceeds the permitted use, you will need to obtain permission directly from the copyright holder. To view a copy of this licence, visit <http://creativecommons.org/licenses/by/4.0/>.

© The Author(s) 2025

Acknowledgements

We thank Dr. Ilka Gehrke and Jan Blömer from Fraunhofer UMSICHT, Oberhausen, for discussing the experimental setup and results with us. We thank the R&D engineers from Hengst SE for sharing their knowledge and